Quantum Electronics **47** (8) 722–729 (2017)

NONLINEAR OPTICAL PHENOMENA https://doi.org/10.1070/QEL16373

Regularities of femtosecond filamentation in the case of superposition of Gaussian and annular laser beams

Yu.E. Geints, A.A. Zemlyanov

Abstract. **The self-action of high-power femtosecond laser beams with a radiation wavelength of 800 nm (formed by superposition of Gaussian and annular beams) in air is theoretically modelled. A detailed analysis of self-focusing and filamentation of this radiation is performed based on the numerical solution of the spectral equation of the unidirectional propagation of a wave packet with allowance for the nonlinearity of the medium, and by tracing averaged diffraction-optical rays. It is shown that, in terms of the diffraction-beam optics, the outer annulus forms a waveguide, which facilitates self-trapping of the central part of the combined beam, supplying the light energy to the filament. The spatial stability of this waveguide depends on the energy stored in the annulus and on the distance from the latter to the beam axis.**

Keywords: *femtosecond filamentation, Gaussian annular laser beams, diffraction-beam optics.*

1. Introduction

The phenomenon of light self-focusing in optical media has been actively investigated since the first half of the 1960s [1–4]. The great interest in this problem is due to the fact that self-focusing of laser beams is a striking manifestation of nonlinear-physics effects, which is of great practical importance for atmospheric optics [5, 6]. The essence of this phenomenon is as follows: at a peak pulse power exceeding some critical level, a self-induced collecting aberration lens is formed on the propagation path due to the optical Kerr effect; this lens focuses the radiation. As a result of this nonlinear focusing, a narrow high-intensity light channel or a group of channels, referred to as filaments, is formed within the beam.

An interesting issue in the study of self-focusing and filamentation of light pulses is the use of shaped beams with a transverse intensity distribution differing from Gaussian. Examples are annular (tubular) [7] and super-Gaussian [8] beams, quasi-diffraction-free Bessel–Gaussian beams [9, 10], Airy beams [11], Mathieu beams [12], and a combination of a Gaussian beam (GB) with an annular beam [13]. The practical importance of shaped beams is related to the specific features of their linear diffraction, which, in turn, opens ways for additional monitoring of the nonlinear propagation (filamentation) zone.

Yu.E. Geints, A.A. Zemlyanov V.E. Zuev Institute of Atmospheric Optics, Siberian Branch, Russian Academy of Sciences, pl. Akad. Zueva 1, 634021 Tomsk, Russia; e-mail: ygeints@iao.ru

Received 21 March 2017; revision received 13 June 2017
Kvantovaya Elektronika **47** (8) 722–729 (2017)
Translated by Yu.P. Sin'kov

A combined beam, which will be considered below, is formed by coherent superposition of the light fields of Gaussian and tubular beams. The transverse intensity distribution in this beam has an isolated central maximum and an annulus around it, which is generally of much lower intensity. Concerning the spatial form of this beam, it is close to one of the low-order radially symmetric modes of the Laguerre–Gauss distribution [14]. In the studies devoted to the filamentation of laser beams, this distribution is referred to as a 'dressed beam' (DB) [13], where the outer annulus plays the role of 'dressing' light. Within the model of a filament as a robust structure, which is dynamically supplied with energy from an external reservoir (at the beam periphery) to compensate for the loss on multiphoton ionisation and generation of a plasma channel in the medium [15, 16], specifically this outer annulus can be considered as an energy source feeding the filament formed by the central part of the beam. Due to this, as was shown in [13, 17], it becomes possible to multiply increase the filamentation length in a DB in comparison with that for a GB of the same radius and power. It was found that the degree of manifestation of this effect increases with increasing energy of the outer annulus and depends on the conditions of its focusing [18].

At the same time, the concept of an energy reservoir that is used to describe the nonlinear DB propagation, although being intuitively clear, does not give a full idea of the filamentation of beams with a complex spatial profile. In this situation, the influence of the linear diffraction effect may be determining for both the evolution of the beam as a whole and for maintaining or terminating the filament existence. Here, the nonlinear evolution of shaped beams with allowance for the complex amplitude–phase interaction between different spatial regions of the beam should be considered in more detail. It is necessary to understand the physical mechanism according to which the axial filament is maintained.

In this study, we consider the filamentation of high-power femtosecond laser DBs with a centre wavelength $\lambda_0 = 800$ nm in air. The single (axial) filamentation of this radiation is theoretically modelled, and the influence of the outer-annulus parameters on the characteristics of the region of maximum laser pulse intensity is investigated. To this end, we apply visualisation of the light wave propagation by tracing diffraction-optical rays [19], i.e., construct trajectories the tangent to which coincides with the Poynting vector direction [20]. Note that a similar approach was previously successfully applied when studying the regularities of the unimodal-beam filamentation [19, 21] and the evolution of radiation in the post-filamentation propagation stage [22]. An analysis of the ray patterns allowed us to put forward a hypothesis explaining the elongation of the axial filament in a DB by not only the

energy transfer from the outer annulus but also (to a greater extent) the self-channelling of the filamented part of the beam in a peculiar 'waveguide channel' formed during the outer annulus propagation.

2. Nonlinear optical model of air and numerical simulation method

Below, we will discuss the results of the numerical simulation of the propagation of high-power femtosecond Ti:sapphire laser pulses with $\lambda_0 = 800$ nm in air. The evolution equation for the optical field of laser pulse in a nonlinear medium is taken to be the equation of unidirectional propagation of the complex field, $E_{k\omega} = E(k_x, k_y, z; \omega)$, in the spatial–temporal frequency domain [23]:

$$\frac{\partial E_{k\omega}}{\partial z} = \mathrm{i}\left(k_z - \frac{\omega}{v_g}\right)E_{k\omega} + \mathrm{i}\frac{\omega^2}{2c^2 k_z}\frac{P_{k\omega}}{\epsilon_0}, \qquad (1)$$

where $k_z = \sqrt{k^2(\omega) - k_\perp^2}$ is the wave propagation constant along the evolution variable z; $k_\perp^2 = k_x^2 + k_y^2$ is the squared modulus of the wave-vector transverse component; $k(\omega) = \omega n(\omega)/c$ is the wave number, which depends on the circular radiation frequency ω and the dispersion of the real part of the refractive index of the medium, $n(\omega)$; ϵ_0 is the permittivity of vacuum; c is the speed of light in vacuum; and $P_{k\omega}$ is the nonlinear polarisation of the medium. This equation is written in the moving (with a group velocity v_g) coordinate system, the origin of which is related to the moving pulse.

Within the nonlinear optical model of the medium in which ultrashort laser pulses propagate, several physical processes whose effect on the light field is decisive are selected. These are the light-induced change in the refractive index of air, $n = n(|E|^2)$, which is taken into account by the instantaneous and inertial components of the optical Kerr effect; the photoionisation of the medium; and the plasma formation. Specific expressions for the physical effects contributing to the nonlinear polarisation can be found, for example, in [24].

Equation (1) is supplemented by the kinetic equation for the density of free electrons, ρ_e, of the laser plasma in the medium:

$$\frac{\partial \rho_e}{\partial t} = W_I(\rho_{nt} - \rho_e) + \alpha_{cas}\rho_e I - \nu_r \rho_e^2, \qquad (2)$$

where W_I is the photoionisation rate; α_{cas} is the impact (cascade) ionisation coefficient; ν_r is the three-body recombination rate of free electrons, which is characteristic of gases and liquids [25]; I is the optical field intensity; and ρ_{nt} is the concentration of neutral molecules (atoms) in the medium. The first term on the right-hand side of this equation takes into account the field type of the ionisation of the medium (multiphoton/tunnel ionisation), while the second term describes the cascade ionisation.

The photoionisation rate W_I was calculated according to the Perelomov–Popov–Terent'ev model [26], which was applied for an air mixture of the composition $O_2:N_2 = 20\%:80\%$ with a total concentration of neutral molecules $\rho_{nt} = 2.5\times10^{19}$ cm^{-3}. The values of other parameters in Eqns (1) and (2) were taken from our previous study [22]. The critical power P_{cr} of self-focusing in air at the wavelength $\lambda_0 = 800$ nm was 3.2 GW. To set the functional dependence $n(\omega)$, we used the Cauchy dispersion formula [27]. Air was assumed to be nonabsorbing.

In the numerical calculations, the initial profile of the transverse amplitude distribution of the laser field with a plane phase front in the coordinates $\boldsymbol{r}_\perp \equiv (x, y)$ was set as a sum of two Gaussian functions:

$$E(\boldsymbol{r}_\perp, z=0) = E_0 \exp\left[-\left(\frac{t}{2t_p}\right)^2\right] \times\left\{\exp\left[-\left(\frac{|\boldsymbol{r}_\perp|}{2R_0}\right)^2\right] + a_r \exp\left[-\left(\frac{|\boldsymbol{r}_\perp - \boldsymbol{r}_r|}{2R_r}\right)^2\right]\right\}, \qquad (3)$$

where R_0 and R_r are, respectively, the radius of the central lobe and the annulus width (at the intensity level of 1/e), $\boldsymbol{r}_r$ is the radius vector of the annular region with a relative amplitude a_r, $E_0 = \sqrt{2I_0/(cn_0\epsilon_0)}$, n_0 is the refractive index of the medium, I_0 is the pulse peak intensity, and t_p is the pulse duration. For definiteness, all calculations were performed for beams with an initial radius $R_0 = 2$ mm at a pulse duration $t_p = 100$ fs. The relative thickness R_r/R_0 of the DB annulus was fixed (0.2), whereas parameters a_r and $\boldsymbol{r}_r$ could be varied. The numerical grid had the following sizes: $R_\perp = 20R_0$ (along the spatial coordinate) and $T = 16t_p$ (along the temporal coordinate), with steps of 10 μm and 2 fs, respectively.

3. Simulation results and discussion

Let us now analyse the results of the numerical calculations of the single filamentation of a laser DB. The influence of the outer annulus on the structure of the filamentation zone is illustrated in Fig. 1, which shows the pulse energy density distribution

$$w(\boldsymbol{r}_\perp, z) = \int_T |E(\boldsymbol{r}_\perp, z; t)|^2 \mathrm{d}t$$

(normalised to the initial value $w_0 \equiv w(\boldsymbol{r}_\perp = 0, z = 0)$) for beams of two types: Gaussian and 'dressed'. The initial peak intensity I_0 was the same in both cases and equals 0.13 TW cm^{-2}, which provided a fivefold excess in the pulse peak power $P_0 = 16$ GW above the critical power P_{cr} for the GB.

As follows from the presented profiles, the GB (Fig. 1a) forms three successive nonlinear focusing zones, beginning with a distance of $z \approx 10$ m and ending with a distance of $z \approx 22$ m, at which the maximum energy density is attained. The length of the GB filamentation zone, calculated from the trace profile of the peak free-electron density in the beam channel (at a level of 10^{14} cm^{-3}), is ~7 m in this case.

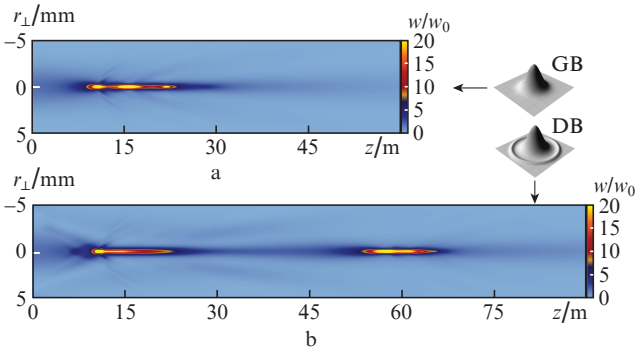

Figure 1. (Colour online) Distribution of the pulse energy density along the path in the cases of the (a) GB and (b) DB filamentation.

Due to the presence of outer annulus, the DB power was approximately twice as large (28 GW); therefore, the first nonlinear focus (and, correspondingly, the filamentation starting point) corresponds to $z = 8$ m (Fig. 1b). Then several more nonlinear beam focusings are implemented, which can arbitrarily be divided into two groups, spaced by ~30 m. The filamentation end corresponds to a distance of $z = 65$ m, which is much larger than that for the GB.

Note that the effect of filament elongation in the DB cannot be explained by only the increase in its initial power with respect to the GB power. Our calculations (omitted in this paper) show that, even when the GB has the same value of P_0 as the annular beam (Fig. 1b), the filament length, despite the elevated power, is only 14 m. This is twice as large as the filamentation length in Fig. 1a but several times smaller than the filamentation length for the DB. Obviously, the reason for the filamentation zone elongation is the peculiar DB profile (specifically, the presence of an outer annulus).

Indeed, the annular region contains a part of the light beam energy and can serve as an additional energy source for central filaments [13]. This possibility is illustrated by Fig. 2, which shows the trace dependences of the maximal achieved (during the pulse) free-electron density $\rho_e(z)$ and the maximum intensity $I_{max}(z)$ on the DB axis at different ratios of the energies of the annulus (E_r) and central lobe (E_c): $\beta = E_r/E_c$. The relative (reduced) peak power $\eta = P_0/P_{cr}$ in the central part of the beam was fixed ($\eta = 5$), and the variation in the energy within the annulus was controlled by the amplitude coefficient a_r.

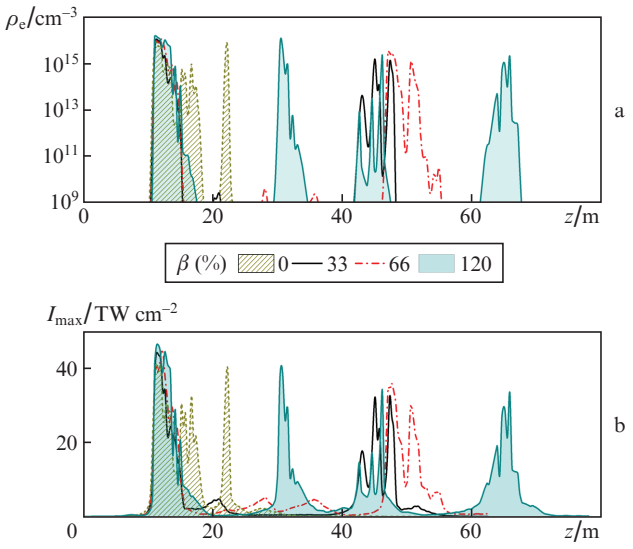

Figure 2. (Colour online) (a) Free-electron density on the axis and (b) peak intensity during the propagation of DBs with different percentages of energy (β) in the annulus.

It can be seen that the increase in energy in the annular region of the beam with respect to the energy in its central maximum, with conservation of the geometric shape and position of the annulus, is accompanied by an elongation of the domain of existence of an enhanced light intensity and plasma electron density. Similar to Fig. 1, this elongation occurs not uniformly along the propagation range but stepwise, in the form of successive beam refocusings. Note that the effect of annulus manifests itself even at a small energy addition to the energy of the beam central lobe ($\beta = 33\%$), immediately doubling the filamentation length due to the occurrence of an additional region of local beam focusing at a distance close to $z = 45$ m.

A further increase in the annulus energy E_r (to $\beta = 66\%$) leads to only a relatively small elongation of the filamentation region, which is due to the displacement of the second refocusing coordinate by approximately 6 m from the beginning of the path. However, at an energy in the annulus exceeding the energy in the central maximum ($\beta = 120\%$), the structure of the filamentation zone sharply changes again. Two more regions of beam refocusing arise at distances of $z \approx 30$ and 65 m. Now all intensity peaks are located in a filament about 70 m long, almost equidistantly with a step of 20 m. Numerical calculations show that, with a further increase in the annulus energy with respect to the energy of the central part, no further significant elongation of the filament is observed. At the same time, the previously formed refocusing regions undergo spatial expansion, and the gaps between them are filled with plasma bunches characterised by a high electron density.

Note that the restructuring of the DB filamentation region and the occurrence of new intensity bursts in this case are in no way related to the filamentation of the annulus field, which occurs, for example, during the self-focusing of femtosecond tubular beams [7, 28]. Although the energy (and power) in the DB annular region can formally be considered as sufficient for implementing its filamentation, especially at $\beta > 50\%$, the annulus is not filamented in reality. This is confirmed by our calculations (omitted in this paper) of the nonlinear propagation of a DB without a central maximum, i.e., an isolated annulus with a peak power up to 30 GW ($\beta \approx 150\%$). Obviously, the physical reason for the absence of nonlinear dynamics for an annular beam is the much higher threshold power necessary for its self-focusing as a whole [7]. According to the estimates, the collapse of an isolated annular beam with the same parameters as in Fig. 1 occurs only at $P_0 > 50$ GW, which is more than an order of magnitude larger than the P_{cr} value for GB.

This rather nontrivial dynamics of the DB self-focusing at a change in the annular region parameters indicates that the outer annulus not only supplies energy to the filament but also affects in a certain way the filamentation of the beam central region due to the specificity of the diffraction of a light beam with the multimodal profile under consideration. This beam initially contains isolated light wave structures (central lobe and annulus), whose fields interfere when propagating in the medium and thus affect the entire process of radiation self-action.

Note that, during the GB filamentation, one can also observe peculiar ring-type energy structures, which are spontaneously organised and can be interpreted within the Fresnel diffraction of unimodal radiation from a self-formed plasma bunch [1]. However, in the case of a DB or, e.g., a Bessel–Gaussian beam [9], these energy rings are present in the initial beam. Their power is generally insufficient for implementing independent filamentation, due to which their influence on self-focusing of the beam central regions can be considered as quasi-linear. Nevertheless, as will be shown below, this effect may radically change the pattern of the beam self-action as a whole.

4. Waveguide analogy of light beam filamentation

Let us consider the transformation of the amplitude–phase profile of a light beam as a result of the interference of the

annulus and filamented centre optical fields, based on the analysis of the evolution of the light wave phase. In geometric optics, phase fronts are generally visualised using the technique of tracing geometric-optics rays [27], which are straight lines (in a homogeneous medium), tangential to the phase-front normal at each point. For a light beam of finite size, a case where the eikonal approximation is violated and the diffraction effects become pronounced during the beam propagation in the medium, the geometric ray should be replaced with the so-called diffraction ray (DR) [19]. In the general case, each DR is a curvilinear trajectory (an integral curve of the spatial component of the light field Poynting vector). DRs are not intersected in accordance with their definition.

Previously we showed [19, 21, 22] that the formalism used in the description of the DRs and related diffraction-ray tubes is adequate for qualitative representation of the data on nonlinear self-action of light beams. This approach makes it possible to visualise a number of peculiar aspects of interaction of the light field with a nonlinear medium, which are related specifically to the transformations of wave phase profile and are not traced in the conventional 'amplitude' representation of the light pulse evolution. Below we will use the diffraction-ray description to analyse the DB filamentation.

According to [22], let us write the governing relations of diffraction-ray optics. The equation for the transverse DR coordinate $\boldsymbol{R}_\mathrm{d}$ has the form

$$\frac{\mathrm{d}^2\boldsymbol{R}_\mathrm{d}}{\mathrm{d}z^2} = \frac{1}{2\varepsilon_0}\nabla_\perp \varepsilon_\mathrm{eff}. \tag{4}$$

Here, ε_eff is the so-called effective permittivity of the medium [29], which can be written as the sum

$$\varepsilon_\mathrm{eff} = \varepsilon_0 + \varepsilon_\mathrm{nl} + \varepsilon_\mathrm{d}, \tag{5}$$

where $\varepsilon_0 = n_0^2$ is the unperturbed permittivity; ε_nl is the nonlinear component, taking into account the refraction action of the Kerr effect and the self-induced electron plasma; $\varepsilon_\mathrm{d} = \Delta_\perp A/(k_0^2 A)$ is the diffraction component; A is the real amplitude of the light field; and $k_0 = 2\pi/\lambda_0$ is the wave number in vacuum.

Using the representation of a complex field in terms of real (slowly varying) amplitude and phase, $E = A\exp(\mathrm{i}\varphi)$, in the steady-state case, one can relate the effective permittivity of the medium, ε_eff, to the optical-wave phase φ as follows:

$$\varepsilon_\mathrm{eff} = \varepsilon_0\left[1 + \frac{2}{k_0}\frac{\partial\varphi}{\partial z} + \frac{1}{k_0^2}(\nabla_\perp\varphi)^2\right]. \tag{6}$$

Then, instead of (4), one can write the following DR equation, which is more convenient for calculations:

$$\frac{\mathrm{d}\boldsymbol{R}_\mathrm{d}}{\mathrm{d}z} = \frac{1}{k_0}\nabla_\perp\varphi, \tag{7}$$

This equation indicates a direct relationship between the DR and the path of the light energy flux, described by the transverse component of Poynting vector $\boldsymbol{S}_\perp$:

$$\nabla_\perp\varphi = \frac{1}{2\mathrm{i}A^2}\left(A^*\nabla_\perp A - A\nabla_\perp A^*\right) = \frac{k_0}{A^2}\boldsymbol{S}_\perp.$$

Below, we will consider the DRs averaged over the pulse time, whose trajectories are calculated from formula (7) with an averaged gradient of the field phase

$$\overline{\nabla_\perp\varphi} = \int\frac{\nabla_\perp\varphi I\,\mathrm{d}t}{w(\boldsymbol{r}_\perp, z)}.$$

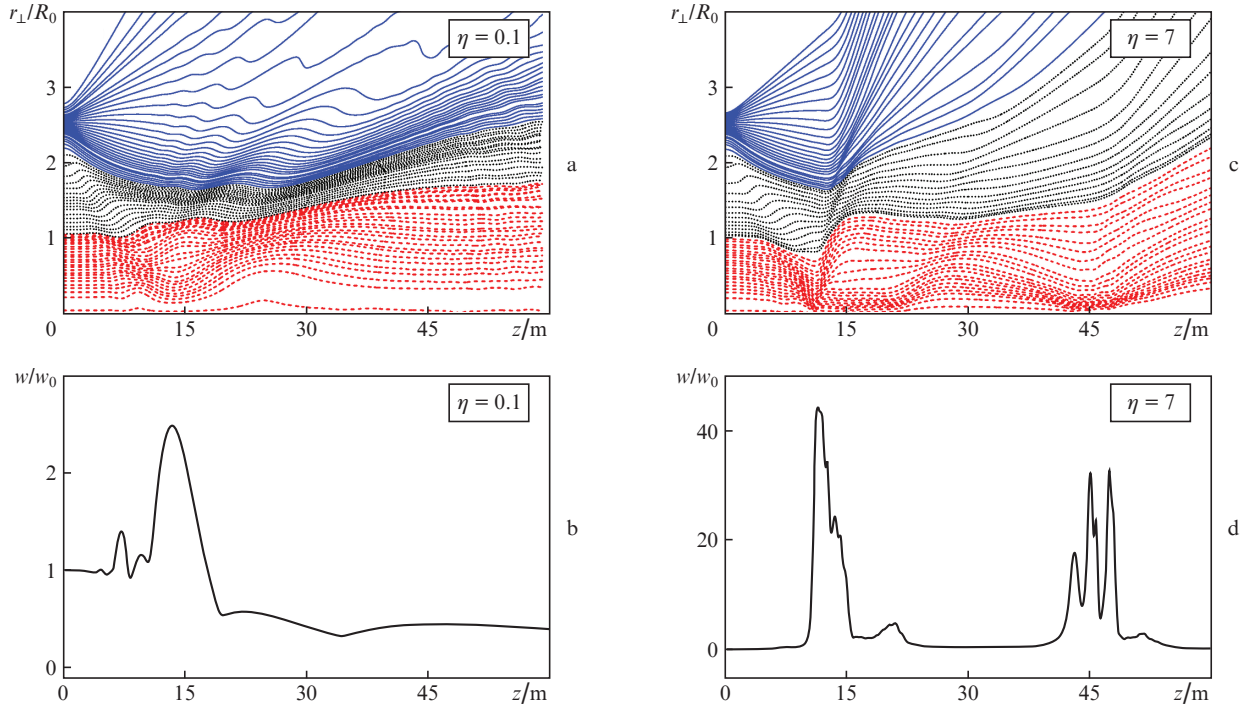

Figure 3. (Colour online) (a, c) Trajectories of averaged DRs and (b, d) the relative light energy density on the beam axis for DBs with different initial powers η.

Let us now analyse the beam trajectories obtained as a result of the joint solution of Eqns (1), (2), and (7) for a DB. The DR path is shown by individual sets of curves in Fig. 3 for beams with different initial powers. The symmetry of the ray pattern with respect to the beam axis makes it possible to construct DRs for only half of the pattern. The corresponding energy density profile w_{max}/w_0 on the beam axis is given directly under each plot with DR trajectories.

First we will consider the ray pattern describing the linear propagation of an annular GB with a subcritical reduced power $\eta = 0.1$ (Fig. 3a). The multimodal intensity profile of the DB can arbitrarily be divided into several structures: the most intense central part, a low-intensity intermediate periphery, and a narrow outer annulus centred at $r_r/R_0 = 2.5$. For convenience of analysis, the DRs corresponding to these structures are shown in Figs 3a and 3c by lines of different types.

Beginning with the starting point, the outer annulus, which has a smaller transverse size than the axial maximum, undergoes the most significant diffraction broadening. Some of the rays, which form the annulus, tend to the beam axis and begin to affect the peripheral DRs, 'pressing' them to the axis. As a result, the light rays of the central region also undergo crowding, which leads, as a result, to the formation of a diffraction focus at $z = 15.2$ m. This focus corresponds to the main maximum in the axial energy density distribution (Fig. 3b).

Central DRs, emerging from the focal waist, acquire the highest angular divergence and begin to press the neighbouring rays from the low-intensity periphery (which have a lower divergence), which, in turn, affect similarly the rays of the outer annulus. As a result, the annulus rays, initially converging to the axis, are first slewed and then become stably divergent from the axis.

Crowding of the peripheral rays occurs also in the rotation zone of annular DRs, due to which the divergence of the central DRs from the axis decreases. As a result, a spatial layer with a thickness on the order of the initial radius of the central part of the beam, R_0, arises inside the beam; the DRs in this layer propagate almost parallel to the axis at a distance exceeding the beam Rayleigh length. As for external manifestations, this behaviour of the rays is similar to the propagation of a light beam in a conventional waveguide. However, in contrast to conventional refraction waveguides, whose principle of operation is based on the guidance of light due to its refraction and reflection from boundaries with air, the self-organised waveguide layer in Fig. 3a does not have physical boundaries. In this case, the 'walls' are the caustic surfaces formed by the crowding of the peripheral DRs. When describing below similar structures, we will use for convenience the term 'diffraction waveguide' (DW), taking into account its field nature. It is noteworthy that this waveguide layer is formed during linear DB propagation (only due to the confining effect of the outer annulus).

Let us now turn to Figs 3c and 3d, which show the ray trajectories and the energy density for a DB of supercritical power ($\eta = 7$). Having compared this pattern with the linear case, one can see that, from the propagation starting point and practically to the diffraction focus, the beam evolution is similar to that in the linear and nonlinear cases. However, then differences arise in the DR trajectories, which are related to the enhancing Kerr self-focusing of the beam central regions; in sum, this leads to the occurrence of the first local nonlinear focus at $z = 13.7$ m.

Since the radial coordinate of rays in the nonlinear-focus region is much smaller (the beam is more strongly compressed) than in the linear waist, the DRs emerge from focus at larger angles. The collisions with the peripheral rays of the beam, which are pressed from above by the annular DRs, stop the tendency of the latter to shift to the axis. Sharp bendings (folds) are formed in the diffraction pattern, which correspond to the conical emission annuli [30] arising in the energy density distribution (Fig. 1b) due to the interference of counterpropagating waves from the nonlinear focus and the beam periphery.

After the first nonlinear focus, the central DRs pass to the channelling regime, in which their radial coordinate is limited by the low-intensity peripheral rays. Some of the DRs, as in the linear case, propagate parallel to the optical axis, and sinusoidal trajectories are observed in the more intense part of the beam; these trajectories are characteristic of a peculiar class of refraction gradient waveguides known as selfocs [31].

In comparison with the ray filamentation picture of a GB (see, for example, [22]), where one can also observe the formation of a selfoc, the diffraction channelling of paraxial DRs in a DB is a property inherent in the latter, which, as was shown above, manifests itself even in the case of conventional linear propagation. With an increase in the DB power, the Kerr self-focusing manifests itself not only in the central maximum but also in the outer annulus, although to a much smaller extent. This effect partially compensates for the diffraction of the annulus field (the annular DRs have a smaller spread in the initial stage) and reduces the divergence of the beam shell of the self-induced diffraction waveguide. Due to this, the high-intensity DB light channel has a larger total length than the GB channel; at the same time, it is characterised by a significantly different intensity distribution.

Using the definition of the effective permittivity of the medium ε_{eff}, one can make a direct analogy between the beam propagation in a real waveguide and in a self-induced DW. The formation of a DW by an annular beam can clearly be observed in Fig. 4, which shows the radial profile of the relative change in the effective permittivity of the medium $\Delta\varepsilon_{eff} = (k_0R_0)^2(\varepsilon_{eff}/\varepsilon_0 - 1)$ along the beam propagation direction. The laser parameters correspond to those in Fig. 3; the calculation was performed using formula (6). Recall that the effective permittivity ε_{eff} differs from the material value ε_0 (which is determined by only the physical structure of the

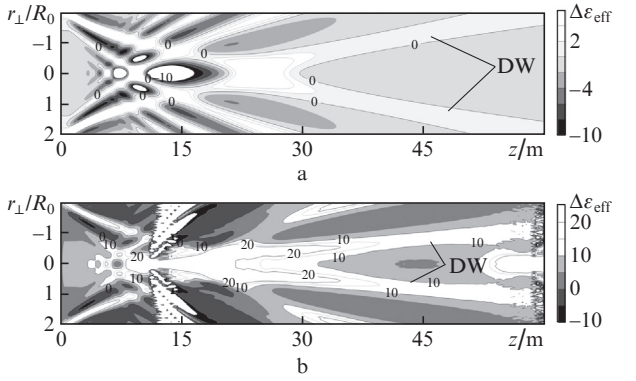

Figure 4. Isolevels of the effective permittivity of the medium during the DB propagation in the (a) linear and (b) nonlinear regimes.

medium) by the presence of a field contribution, related to the change in the amplitude and phase of optical wave during its propagation.

It can be seen that $\Delta\varepsilon_{\text{eff}}$ along the path may take both positive and negative values, due to which a peculiar pattern of effective permittivity is formed in the beam. The diffraction rays, as well as conventional geometric-optics rays, being refracted at a boundary between regions with different $\Delta\varepsilon_{\text{eff}}$ values, bend towards higher effective permittivities. The diffraction waveguide is formed by the region with a weakly changing $\Delta\varepsilon_{\text{eff}}$, surrounded by optically denser walls; the gradient of effective permittivity is negative at the external boundaries of these walls. Specifically this circumstance provides the radiation channelling in this light structure.

A light ray entering this DW will be held by optically dense walls at a certain distance. In contrast to a conventional refraction waveguide with a hollow core, where geometric-optics rays are reflected from the external boundary, the DRs arriving at the DW wall are refracted towards larger $\Delta\varepsilon_{\text{eff}}$ values; i.e., tend to stay in the DW. A diffraction ray may leave this waveguide only at certain angle of incidence on the waveguide wall. This may occur either when a DR emerges from the focal region, where large $|\nabla_\perp\varepsilon_{\text{eff}}|$ values are implemented and DRs are significantly bent, or when the waveguide walls are insufficiently dense (small $|\nabla_\perp\varepsilon_{\text{eff}}|$ values). The regions with these waveguide properties are indicated in Fig. 4; note that a DW is formed in both cases: upon linear propagation of DB and its filamentation. In the latter case, the DW has a smaller cross section and 'higher' walls (the $\Delta\varepsilon_{\text{eff}}$ values are larger).

Note that one of the first physical models of Gaussian laser pulse filamentation was the model of a hollow refraction waveguide [32] [where the term ε_{d} in (5) is disregarded], formed by radiation propagating in a medium as a result of the competition of nonlinear Kerr effects and plasma defocusing. Indeed, as follows from our calculations (omitted in this paper), when considering the GB filamentation in terms of the effective permittivity of the medium, one can also trace the formation of a peculiar waveguide structure, similar to the above-described DW in a DB. However, in the case of GB, a DW is formed directly on the beam axis and, in contrast to the refraction waveguide [32], does not contain any hollow core with a low refractive index.

Figure 5 shows how the distance between the outer annulus and the beam axis affects the stability and length of self-induced DW. Here, DBs with the same power but different parameters r_{r} are compared. It can be seen that, before the first nonlinear focus, the ray patterns of the central part of the beam do not exhibit any significant differences, and the self-focusing of the centre is not affected by the annulus. However, emerging from the focus, the DRs in a beam with an annulus of larger radius (Fig. 5a) meet the peripheral DRs, which have not been pressed sufficiently well by the outer annulus rays. Therefore, most of peripheral DRs move away (jointly with the annulus rays) from the axis, whereas the rest form a short waveguide channel. This channel degrades after three more refocusings of axial DRs, because it does not undergo a proper diffraction pressing by the peripheral rays.

Vice versa, when the annulus is located closer to the beam centre (Fig. 5c), it begins to affect earlier the central DRs, which manifests itself in the smaller coordinate of the nonlinear focus ($z \approx 9$ m) and in the formation of a DW with a narrower cross section than in the previous cases. In this situation, the ray trajectories are characterised by the most regular behaviour along the path, because the force of the diffraction pressing of annulus, f_{d}, is lower in this case [19]: $f_{\text{d}} = |\nabla_\perp\varepsilon_{\text{d}}| \propto r_{\text{r}}/R_{\text{r}}^2$. Nevertheless, a thinner DW (for a DB

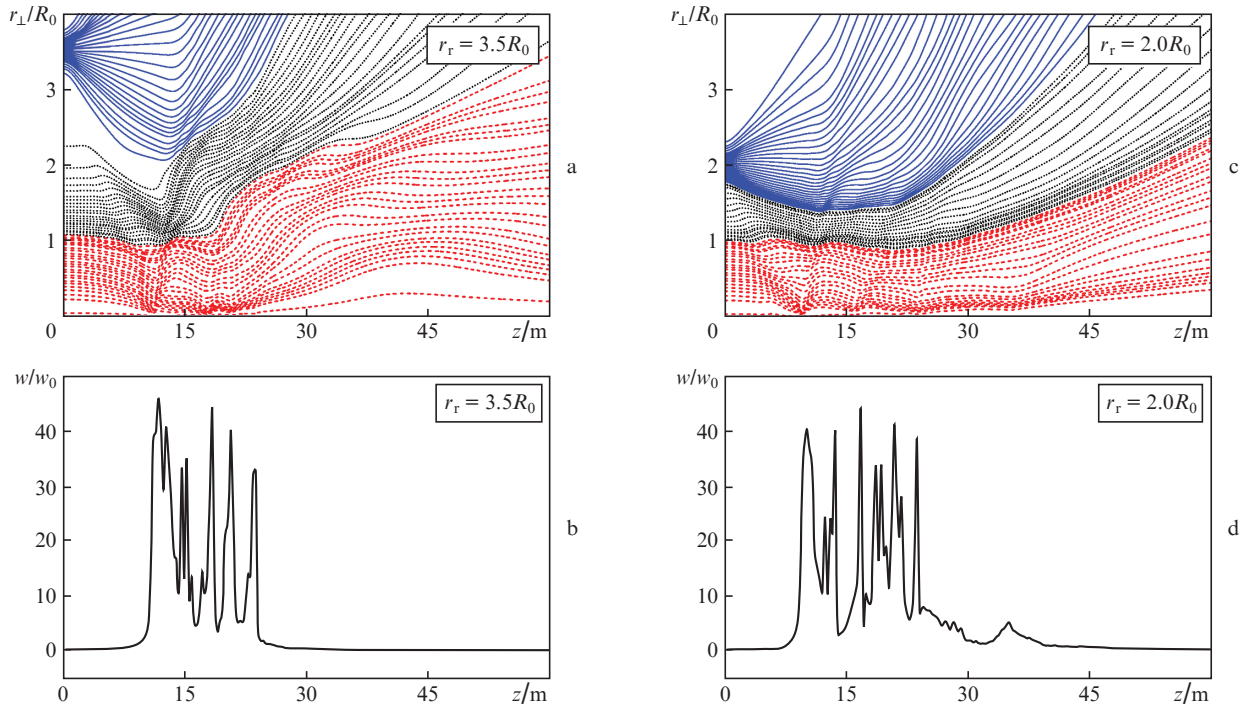

Figure 5. (Colour online) The same as in Fig. 3 but for DBs with different annulus positions, r_{r}.

with an annulus located at $r_r = 2.5R_0$) decomposes more rapidly and does not provide such a long filamentation as in the case of $r_r = 2.5R_0$.

This fact indicates that the most optimal position of the outer annulus is that in which the effect of annulus rays is the strongest at the instant when the central DRs emerge from the nonlinear focus. Applying the relations for the GB diffraction optics [27] and the theory of aberration-free self-focusing [20], one can easily derive an expression for the optimal position r_r of the outer annulus:

$$r_r \approx R_0^2 / \left[R_r \sqrt{\eta^* - 1} \right],$$

where η^* is the effective reduced pulse power, i.e., the peak power corrected for the inertia of the Kerr effect. For example, for the above-considered case of emission of a pulse with $\eta = 7$, this correction yields $\eta^* = 4.6$, which leads to the optimal position of an annulus with $R_r/R_0 = 0.2$ at a distance of $r_r \approx 2.65R_0$.

Thus, when a DB is used to form an extended filamentation zone, important factors are not only the amount of energy in the outer annulus (see Fig. 2) but also the choice of the annulus position in correspondence with the pulse power and the size parameters of the entire beam.

5. Conclusions

We considered one of the ways to control the length and structure of the filamentation zone with the aid of high-power ultrashort laser radiation by varying the shape of the light beam at the input of a nonlinear medium. Based on the numerical solution of the spectral equation of unidirectional propagation of light pulses, we theoretically investigated the regularities of the self-action in air for femtosecond radiation with a combined intensity profile, composed of an intense axial beam of maximum intensity, surrounded by a low-intensity annulus of larger radius (DB [13]). The interference of the linear and nonlinear physical mechanisms during the self-focusing and filamentation of this radiation was analysed in detail by constructing time-averaged diffraction-ray patterns.

It was established that the most important advantage of the use of DBs in problems of laser beam propagation is the possibility of significant elongation of the filamentation zone in a medium, with energy consumption comparable with the GB energy. For example, for a DB of millimetre radius with a gigawatt pulsed power, the length of the filamentation zone may increase almost three times in comparison with that for a GB of the same energy. It was found that, during the pulse filamentation, the outer annulus does not only play the role of an energy reservoir for maintaining the axial filament. An analysis of ray trajectories showed that a specific feature of the nonlinear DB propagation is the greater importance of the diffraction mechanisms, as well as the interference of the optical fields of central and annular regions during the pulse self-action. In this context, the presence of an outer annulus leads to the formation of a peculiar effective permittivity profile near the beam (or DW) axis, facilitating the self-trapping of the central part of the beam and holding it within the longitudinal boundaries of the filament. The stability and length of this DW are affected (increased) by the energy in the annulus and its spatial position with respect to the beam axis.

Acknowledgements. We are grateful to V.P. Kandidov for the fruitful discussion and valuable remarks during the preparation of the paper.

Yu.E. Geints and A.A. Zemlyanov acknowledge the support of the Russian Science Foundation (Contract Nos 16-17-10128 and 15-17-10001, respectively).

References

1. Shen Y.R., Boyd R.W., Lukishova S.G. (Eds) *Self-Focusing: Past and Present* (Amsterdam: Springer, 2009).
2. Couairon A., Myzyrowicz A. *Phys. Rep.*, **441**, 47 (2007).
3. Berge L., Skupin S., Nuter R., Kasparian J., Wolf J.-P. *Rep. Prog. Phys.*, **70**, 1633 (2007).
4. Chekalin S.V., Kandidov V.P. *Phys. Usp.*, **56**, 123 (2013) [*Usp. Fiz. Nauk*, **183**, 133 (2013)].
5. Kasparian J., Rodriguez M., Mejean G., Yu J., Salmon E., Wille H., Bourayou R., Frey S., Andre Y.-B., Mysyrowicz A., Sauerbrey R., Wolf J.-P., Wöste L. *Science*, **301**, 61 (2003).
6. Mechain G., Amico C.D., Andre Y.-B., Tzortzakis S., Franco M., Prade B., Mysyrowicz A., Couairon A., Salmon E., Sauerbrey R. *Opt. Commun.*, **247**, 171 (2005).
7. Geints Yu.E., Zemlyanov A.A. *Opt. Atmos. Okeana*, **26**, 647 (2013).
8. Grow T.D., Ishaaya A.A., Vuong L.T., Gaeta A.L. *Opt. Express*, **14**, 5468 (2006).
9. Roskey D.E., Kolesik M., Moloney J.V., Wright E.M. *Opt. Express*, **15**, 9893 (2007).
10. Kompanets V.O., Chekalin S.V., Kosareva O.G., Grigor'evskii A.V., Kandidov V.P. *Quantum Electron.*, **36** (9), 821 (2006) [*Kvantovaya Elektron.*, **36** (9), 821 (2006)].
11. Panagiotopoulos P., Papazoglou D.G., Couairon A., Tzortzakis S. *Nat. Commun.*, **4**, 2622 (2013).
12. Hu Y., Nie J., Sun K., Dou X., Chen X., Wan L. *J. Mod. Opt.*, **64**, 572 (2017).
13. Mills M., Christodoulides D., Kolesik M. *Opt. Lett.*, **38**, 25 (2013).
14. Abramochkin E.G., Volostnikov V.G. *J. Opt. A: Pure Appl. Opt.*, **6**, 5157 (2004).
15. Mlejnek M., Wright E.M., Moloney J.V. *Opt. Lett.*, **23**, 382 (1998).
16. Liu W., Gravel J.-F., Théberge F., Becker A., Chin S.L. *Appl. Phys. B*, **80**, 857 (2005).
17. Scheller M., Mills M.S., Miri M.-A., Cheng W., Moloney J.V., Kolesik M., Polynkin P., Christodoulides D.N. *Nat. Photonics*, **8**, 297 (2014).
18. Mills M., Heinrich M., Kolesik M., Christodoulides D. *J. Phys. B*, **48**, 094014 (2015).
19. Zemlyanov A.A., Bulygin A.D., Geints Yu.E. *Opt. Atmos. Okeana*, **24**, 839 (2011).
20. Akhmanov S.A., Sukhorukov A.P., Khokhlov R.V. *Sov. Phys. Usp.*, **10**, 609 (1968) [*Usp. Fiz. Nauk*, **93**, 19 (1967)].
21. Zemlyanov A.A., Bulygin A.D., Geints Yu.E. *Opt. Atmos. Okeana*, **26**, 350 (2013).
22. Zemlyanov A.A., Bulygin A.D., Geints Yu.E. *Opt. Atmos. Okeana*, **29**, 359 (2016).
23. Kolesik M., Moloney J.V. *Phys. Rev. E*, **70**, 036604 (2004).
24. Couairon A., Brambilla E., Corti T., Majus D., de J. Ramírez-Góngora O., Kolesik M. *Eur. Phys. J. Spec. Top.*, **199**, 5 (2011).
25. Raizer Yu.P. *Gas Discharge Physics* (New York: Springer, 1991).
26. Perelomov A.M., Popov V.S., Terent'ev M.V. *JETP*, **23**, 924 (1966) [*Zh. Eksp. Teor. Fiz.*, **50**, 1393 (1966)].

27. Born M., Wolf E. *Principles of Optics: Electromagnetic Theory of Propagation, Interference, and Diffraction of Light* (Oxford: Pergamon, 1964; Moscow: Nauka, 1973).
28. Vasil'ev E.V., Shlenov S.A. *Quantum Electron*., **46**, 1002 (2016) [*Kvantovaya Elektron.*, **46**, 1002 (2016)].
29. Talanov V.I. *Pis'ma Zh. Eksp. Teor. Fiz.*, **2**, 218 (1965).
30. Kandidov V.P., Kosareva O.G., Brodeur A., Chien C.Y., Chin S.L. *Opt. Lett*., **22**, 1332 (1997).
31. Mikaelyan A.L. *Opt. Spektrosk.*, **44** (2), 370 (1978).
32. Nibbering E.T.J., Curley P.F., Grillon G., Prade B.S., Franco M.A., Salin F., Mysyrowicz A. *Opt. Lett*., **21**, 62 (1996).